Published in final edited form as:
Cell. 2010 August 20; 142(4): 568–579. doi:10.1016/j.cell.2010.07.015.

Structural basis for negative cooperativity in growth factor binding to an EGF receptor

Diego Alvarado[1,2], **Daryl E. Klein**[1,3], and **Mark A. Lemmon**[1,4]

[1] Department of Biochemistry and Biophysics, University of Pennsylvania School of Medicine, Philadelphia, PA 19104-6059, U.S.A

SUMMARY

Transmembrane signaling by the epidermal growth factor receptor (EGFR) involves ligand-induced dimerization and allosteric regulation of the intracellular tyrosine kinase domain. Crystallographic studies have shown how ligand binding induces dimerization of the EGFR extracellular region, but cannot explain the 'high-affinity' and 'low-affinity' classes of cell-surface EGF-binding sites inferred from curved Scatchard plots. From a series of crystal structures of the Drosophila EGFR extracellular region, we show here how Scatchard plot curvature arises from negatively cooperative ligand binding. The first ligand-binding event induces formation of an asymmetric dimer with only one bound ligand. The unoccupied site in this dimer is structurally restrained, leading to reduced affinity for binding of the second ligand, and thus negative cooperativity. Our results explain the cell-surface binding characteristics of EGF receptors, and suggest how individual EGFR ligands might stabilize distinct dimeric species with different signaling properties.

INTRODUCTION

Receptor tyrosine kinases (RTKs) in the EGF receptor (EGFR/ErbB/HER) family play pivotal roles in animal development and in disease (Hynes and MacDonald, 2009; Jorissen et al., 2003; Shilo, 2005). In particular, EGFR and ErbB2/HER2/Neu are mutated or overexpressed in several human cancers (Hynes and MacDonald, 2009; Sharma et al., 2007). These facts have motivated the development of tyrosine kinase inhibitors (erlotinib, gefitinib and lapatinib) and monoclonal antibodies (including trastuzumab and cetuximab) used to target these receptors in cancer patients, plus intensive efforts to understand their signaling mechanisms.

Although it is well known that EGF induces dimerization of its receptor (Yarden and Schlessinger, 1987), precisely how this leads to EGFR activation is not yet fully understood (Jura et al., 2009; Lemmon, 2009). Crystal structures of unligated ErbB receptor extracellular regions (Ferguson, 2008) and of ligand-bound dimers of the EGFR extracellular region (Garrett et al., 2002; Ogiso et al., 2002) have revealed large conformational changes that are crucial for ligand-induced dimerization. A key

[4]Address correspondence to: Mark A. Lemmon, Dept. Biochemistry and Biophysics, University of Pennsylvania School of Medicine, 809C Stellar-Chance Laboratories, 422 Curie Boulevard, Philadelphia, PA 19104-6059, U.S.A., Tel: (215) 898-3072, Fax: (215) 573-4764, mlemmon@mail.med.upenn.edu.
[2]Present address: Kolltan Pharmaceuticals, Inc., New Haven, CT 06511, U.S.A.
[3]Present address: Laboratory of Structural Cell Biology, Harvard Medical School, Boston, MA 02115, U.S.A

'dimerization arm' is buried by an intramolecular 'tether' in the unligated receptor (Bouyain et al., 2005; Cho and Leahy, 2002; Ferguson et al., 2003) and becomes exposed in the ligand-bound 'extended' configuration, allowing it to mediate the majority of receptor-receptor interactions in the dimer (Garrett et al., 2002; Ogiso et al., 2002).

Disappointingly, all binding/dimerization models derived from the crystal structures of EGFR extracellular regions (Burgess et al., 2003; Klein et al., 2004) fail to account for the characteristic curvilinear (concave-up) Scatchard plots that were first described for EGF binding to its cell-surface receptor 30 years ago (Magun et al., 1980; Shoyab et al., 1979). These concave-up Scatchard plots can signify either negative cooperativity or heterogeneity of binding sites. Traditionally, the latter interpretation has been assumed for EGFR – leading to the notion that this single gene product gives rise to independent (and much-discussed) 'high-affinity' (K_D ~ 0.3 nM) and 'low-affinity' (K_D ~ 2 nM) classes of EGF-binding site at the cell surface (Schlessinger, 1986). The molecular differences between these proposed classes of binding site, and how they could arise from a single EGF receptor protein, are far from clear. Recent data argue that Scatchard plot curvature reflects negative cooperativity rather than distinct classes of binding site (Macdonald and Pike, 2008; Macdonald-Obermann and Pike, 2009). Neither view can be reconciled, though, with published biophysical studies of the isolated human EGFR extracellular region (s-hEGFR), and several reports have invoked a requirement for other unknown cellular components (Klein et al., 2004; Wofsy et al., 1992).

Here, we describe the structural basis for negatively cooperative ligand binding to an isolated EGFR extracellular region, revealing how this can occur in the absence of other cellular components – as an intrinsic property of the receptor. Our studies exploit the finding that – unlike its human counterpart – the EGF receptor from *Drosophila melanogaster* (dEGFR) retains negative cooperativity in ligand binding (and concave-up Scatchard plots) when its extracellular region is studied in isolation. Because the dEGFR extracellular region (s-dEGFR) retains key ligand-binding characteristics previously seen only for intact EGF receptors in cell membranes, it provides a unique opportunity to understand their structural basis. We describe crystal structures of s-dEGFR bound to its growth factor ligand Spitz, which show how occupying one binding site in a receptor dimer impairs ligand-binding to the second site in an asymmetric complex – providing a structural explanation for the origin of negative cooperativity. Our structures allow us, in effect, to visualize directly the long sought-after 'high-affinity' and 'low-affinity' ligand binding sites of an EGFR family member (although they are not independent). These findings also have important implications for understanding how EGFR ligands with different receptor-binding affinities may elicit distinct sets of cellular responses.

RESULTS AND DISCUSSION

The Ligand-Induced Dimer of the dEGFR Extracellular Region is Asymmetric

The key to understanding negatively cooperative growth factor binding to the *Drosophila* EGF receptor lies in the asymmetry of the Spitz-induced s-dEGFR dimer shown in Figure 1A. We crystallized a form of s-dEGFR bound to the EGF-like domain of Spitz ($Spitz_{EGF}$, encompassing residues 48–105), and determined its structure to 3.2 Å resolution (Table S1). The overall domain architecture of s-dEGFR is very similar to that in human EGFR (Burgess et al., 2003), with which it shares 39% sequence identity over domains I to IV. The 'solenoid' domains I and III both contact the same bound growth factor molecule in ligand-stabilized dimers of *Drosophila* (Figure 1A) and human (Figure 1B) sEGFR. Domains II and IV are cysteine-rich laminin-related domains, and domain II harbors the 'dimerization arm' that drives core receptor • receptor contacts in both dimers. The complete dEGFR extracellular region contains an additional cysteine-rich domain of ~150 amino acids that is

absent in hEGFR (domain V, which resembles domains II and IV). Previous small-angle X-ray scattering (SAXS) studies of s-dEGFR showed that domain V projects as a linear extension from the domain IV C-terminus (Alvarado et al., 2009). Removing domain V (to yield s-dEGFRΔV) was essential for crystallization of the ligand • receptor complexes reported here.

Whereas ligand-bound dimers of the human EGFR extracellular region (Figure 1B) are symmetric, the $(Spitz_{EGF})_2$ • $(s\text{-}dEGFR\Delta V)_2$ dimer shows clear asymmetry (Figure 1A). This asymmetry is most evident at the dimer interface, close to the domain II amino-terminus (marked with an asterisk in Figure 1A). Indeed, significant differences in the relationships between domains I, II, and III are seen when the two subunits from the s-dEGFRΔV dimer are overlaid in Figure 1C (the left-hand molecule from Figure 1A is colored green, and the right-hand molecule is red) – yielding an overall rms deviation in Cα positions of 3.4 Å. Figure 1D further shows that the right-hand molecule of the $(Spitz_{EGF})_2$ • $(s\text{-}dEGFR\Delta V)_2$ complex (red) closely resembles the unligated s-dEGFRΔV structure (cyan) that we recently described (Alvarado et al., 2009), overlaying with Cα position rms deviation of just 1.3 Å. Ligand binding has therefore not altered the domain I/III relationship in the right-hand molecule of Figure 1A. Direct interactions between these two ligand binding domains that stabilize the unligated conformation are retained – but remodeled in detail (Figure S1). By contrast, upon binding to the left-hand subunit (green in Figure 1C), $Spitz_{EGF}$ 'wedges' itself between the two ligand-binding domains, and pushes them apart as indicated by the double-headed arrow in Figure 1C to break the direct domain I/III interactions seen in unligated s-dEGFRΔV (Figures S1A and S1C). Moreover, separating domains I and III with this 'ligand wedge' distorts domain II (which connects them) and forces a substantial reorientation of the dimerization arm (Figure 1C). By distorting domain II in only one of the two s-dEGFRΔV molecules in the dimer (the left-hand one), ligand binding induces the marked asymmetry seen in Figure 1A, and allows formation of a more extensive (asymmetric) dimer interface than would otherwise be possible. Indeed, as described in detail later, the asymmetric dimer interface in Figure 1A buries a total surface area of 3,396 $Å^2$, some 33% greater than the 2,553 $Å^2$ buried between the two nearly-identical subunits of the symmetric human s-EGFR dimer (which overlay with a Cα position rms deviation of just 0.8 Å as shown in Figure 1E).

Inequivalence of the Two Ligand-Binding Sites in the dEGFR Dimer Suggests Cooperativity

One important consequence of asymmetry in the $(Spitz_{EGF})_2$ • $(s\text{-}dEGFR\Delta V)_2$ dimer is that the two ligand-binding sites differ significantly from one another (Figure 2A), whereas the two binding sites in the human s-EGFRΔIV dimer are almost identical (Figure 2B). Differences between the two ligand-binding sites in the $(Spitz_{EGF})_2$ • $(s\text{-}dEGFR\Delta V)_2$ dimer are most apparent where $Spitz_{EGF}$ contacts domain I. Figure 2A shows the two s-dEGFRΔV molecules from Figure 1A overlaid using the bound ligand as reference (the left-hand molecule from Figure 1A is colored green, and the right-hand molecule red). By 'wedging' domains I and III apart, $Spitz_{EGF}$ has shifted domain I of the green molecule towards the top left corner of the figure by 3–5 Å compared with its position in the red s-dEGFRΔV molecule, and has displaced the N-terminal αhelix of domain I by ~7 Å along its axis (see green arrows in Figure 2A). Because of this shift in domain I position, its interactions with $Spitz_{EGF}$ are significantly altered in detail when the red and green sites are compared (upper inset in Figure 2A), although they involve similar sets of dEGFR residues.

The domain III/$Spitz_{EGF}$ interface is less altered between the two binding sites (lower inset of Figure 2A). The change in domain III position with respect to bound ligand is small, and is mostly compensated for by small adjustments in rotamer positions of interfacial side-chains. In a few cases, dEGFR side-chains appear to replace one another functionally in the

two domain III/Spitz$_{EGF}$ interfaces. For example, in the interface between Spitz$_{EGF}$ and the green binding site, the H433 side-chain (underlined in Figure 2A) assumes the position occupied by E460 in the red binding site. Similarly, E400 substitutes spatially for S401 when the Spitz$_{EGF}$-binding surfaces of the green and red binding sites are compared (Figure 2A, lower inset).

These differences in the way that Spitz$_{EGF}$ interacts with the two binding sites in the asymmetric s-dEGFRΔV dimer can also be thought of as a displacement of ligand on the domain I and III surfaces, as illustrated in Figure S2. In this view, it is clear that the Spitz$_{EGF}$ A-, B-, and C-loops all make significantly different contacts with the receptor in the two binding sites. Only the location of the Spitz$_{EGF}$ C-terminus on domain III is fixed between the two sites (Figure S2B), consistent with previous studies that point to the C-termini of other EGF-like ligands as major determinants of binding affinity (Groenen et al., 1994).

As mentioned above, the red binding site in Figure 2A reflects s-dEGFRΔV in a conformation that is unchanged from the unligated receptor (Figure 1D), whereas forming the green binding site requires the ligand to wedge apart domains I and III. When Spitz$_{EGF}$ binds to the green (wedged open) site, a total surface area of 4,030 Å^2 is buried, compared with just 3,730 Å^2 in the red (unaltered) site. Moreover, binding to the green site involves four additional predicted hydrogen bonds between ligand and receptor (an increase of 16% over the red site). Thus, the green s-dEGFRΔV molecule shown in Figures 1C and 2A (the left-hand subunit in Figure 1A) has characteristics expected for a higher affinity site. By contrast, the red s-dEGFRΔV molecule in Figures 1C and 2A (the right-hand subunit in Figure 1A) appears to be restrained in an unligated-like conformation, which may in turn compromise ligand binding so that this site has a lower binding affinity.

Negatively Cooperative Ligand Binding can be Recapitulated with s-dEGFR

The structural inequivalence of the two Spitz$_{EGF}$ binding sites in Figures 1 and 2 prompted us to ask whether distinct classes of binding site (or negative cooperativity) can be detected in studies of Spitz$_{EGF}$ association with the isolated dEGFR extracellular region. We linked s-dEGFR molecules via their flexible C-termini to a solid support to approximate their arrangement at the cell surface while allowing dimerization. An AviTag sequence was introduced (via a unstructured linker) at the s-dEGFR C-terminus to allow enzymatic biotinylation of the protein and its capture on the surface of streptavidin-coated 96 well plates (see Experimental Procedures). Spitz$_{EGF}$ was labeled with Alexa Fluor-488 to monitor its binding to surface-bound s-dEGFR. The representative binding curve in Figure 3A cannot be fit satisfactorily with a simple hyperbola, but fits well to the Hill equation (red curve) with a low Hill coefficient (n_H) of 0.31 that suggests negative cooperativity (the mean n_H value for all experiments was 0.38±0.07, with a microscopic dissociation constant of 49.5 nM). Transformation of these data into a Scatchard plot (Figure 3B) also reveals characteristic concave-up curvature of the sort seen for human EGF binding to its intact receptor at the cell surface. Parallel experiments using a non-dimerizing s-dEGFR mutant confirm that this behavior requires s-dEGFR dimerization, and showed simple hyperbolic binding curves (Figure 3C) and linear Scatchard plots (Figure 3D) with a best-fit n_H value of 1.02 (0.97±0.1 over all experiments) and a K_D value of 0.92 μM.

Our studies of Spitz$_{EGF}$ binding to dimerization-competent s-dEGFR that has been purified to homogeneity are consistent with the negative cooperativity seen for human EGF binding to its intact cell surface receptor (Macdonald and Pike, 2008; Wofsy et al., 1992). Importantly, whereas isolating the human EGFR extracellular region abolishes Scatchard plot curvature (Lax et al., 1991; Lemmon et al., 1997; Livneh et al., 1986; Odaka et al., 1997), our results show that this is not the case for *Drosophila* EGFR. Concave-up

Scatchard plots do not prove negative cooperativity, however. Indeed, the curves in Figure 3A and B can alternatively be fit by assuming the superposition of two hyperbolae that correspond to distinct (and independent) classes of binding site – as has traditionally been done for EGF binding to its cell-surface receptor. In such a fit for Figures 3A/B, a high-affinity site (K_D ~ 4.7nM) could account for ~65% of the saturated $Spitz_{EGF}$ binding signal, and an independent lower-affinity class of sites (K_D ~ 1.3μM) could account for the rest. It seems unlikely that molecular heterogeneity is responsible for the Scatchard plot curvature seen for s-dEGFR. Indeed, these experiments were performed with highly purified protein. Moreover, data in Figures 3C and D for dimerization-defective s-dEGFR$^{dim\text{-}arm}$ argue that dimerization of the dEGFR extracellular region is required for Scatchard plot curvature. Taken together, these findings support the hypothesis that (as for EGF binding to hEGFR) the binding curves in Figures 3A and B represent negatively cooperative binding of $Spitz_{EGF}$ to s-dEGFR dimers, as suggested independently by the features of the asymmetric $(Spitz_{EGF})_2$ • $(s\text{-}dEGFR\Delta V)_2$ dimer structure (and binding-site inequivalence) discussed above. It is also important to note that, both for s-dEGFR in our studies (Figure 3) and for intact EGFR in cells (Macdonald and Pike, 2008), dimerization is required for the appearance of high-affinity ligand binding and for the manifestation of negatively cooperative ligand binding.

Half-of-the-Sites Reactivity in a Spitz • s-dEGFRΔV Crystal Structure

Intriguingly, we also obtained evidence for half-of-the-sites reactivity – the extreme of negative cooperativity – in crystallographic studies of s-dEGFRΔV bound to a variant of $Spitz_{EGF}$ ($Spitz_{EGF\Delta C}$) with a C-terminal truncation that reduces its affinity for the receptor by ~12-fold (Figure S3). Crystals that diffracted to 3.4 Å grew from a 1:1.2 mixture of s-dEGFRΔV and $Spitz_{EGF\Delta C}$, and molecular replacement (MR) identified excellent solutions for two s-dEGFRΔV molecules in the asymmetric unit. One was found using unligated s-dEGFRΔV (or the right-hand molecule in Figure 1A) as the search model. The other could only be found in MR searches using the left-hand s-dEGFRΔV molecule from Figure 1A in which domains I and III are wedged apart. Unfortunately, a marked anisotropy in all datasets made full refinement of this structure impossible. We therefore used only rigid-body refinement, treating each domain of the two s-dEGFRΔV molecules as an independent body (see Experimental Procedures). For domains I and III, this seems well justified by the absence of ligand-induced structural changes in the individual domains of dEGFR or other ErbB receptors (Ferguson, 2008). For domains II and IV, major structural changes may be missed with this approach – but we do not expect them.

The rigid-body refined structure of the s-dEGFRΔV/$Spitz_{EGF\Delta C}$ complex (Figure 4A) suggests a dimer with the same asymmetric arrangement of receptor molecules as seen in the $(Spitz_{EGF})_2$ • $(s\text{-}dEGFR\Delta V)_2$ dimer discussed above, despite the fact that the crystal packing is quite different in the two cases. Most importantly, whereas one receptor molecule showed clear electron density for bound ligand in $2F_o\text{-}F_c$ maps (Figure 4B), the other showed none (Figure 4C) – even at very low contour levels. The absence of ligand from this second site cannot be explained by competing crystallization contacts. Thus, $Spitz_{EGF\Delta C}$ appears to induce the formation of a singly-ligated asymmetric s-dEGFRΔV dimer in these crystals, depicted in Figure 4A. The left-hand (ligated) molecule in Figure 4A has the same conformation as the left-hand molecule in the $(Spitz_{EGF})_2$ • $(s\text{-}dEGFR\Delta V)_2$ dimer in Figure 1A, with domains I and III wedged apart by the bound $Spitz_{EGF\Delta C}$. The right-hand molecule in Figure 4A has the same conformation as unligated s-dEGFRΔV, and its binding site is empty (or at least has very low occupancy). In parallel studies with Vein, a weak dEGFR activator (Schnepp et al., 1998) with binding affinity even lower than that of $Spitz_{EGF\Delta C}$ (data not shown), we determined a 3.4 Å rigid body-refined structure that also shows a singly-occupied asymmetric dimer. These apparently singly-ligated s-dEGFRΔV dimers

suggest half-of-the-sites reactivity, where binding of $Spitz_{EGF\Delta C}$ (or $Vein_{EGF}$) to one site in the s-dEGFRΔV dimer prevents (or greatly impairs) ligand binding to the second site.

Remodeling of the s-dEGFR Dimer Interface upon Ligand Binding

Unlike its human counterpart, the dEGFR extracellular region dimerizes even in the absence of ligand, albeit weakly (K_D ~40 μM). Moreover, unligated s-dEGFRΔV crystallizes as a symmetric (crystallographic) dimer, illustrated in Figure 5A (Alvarado et al., 2009). The interface of this symmetric dimer involves only the domain II dimerization arm, and the N-terminal parts of domain II are splayed apart (Figures 5A, B). The total surface area buried in the unligated dimer interface is just 2,262 $Å^2$.

Binding of $Spitz_{EGF}$ (or $Spitz_{EGF\Delta C}$) enhances s-dEGFR dimerization by approximately 30-fold (Alvarado et al., 2009), associated with an increase of more than 50% in the surface area buried at the dimer interface (to 3,396 $Å^2$). This large expansion of the interface arises primarily from direct contacts between the domain II amino-terminal regions that are seen only in the asymmetric ligand-induced dimer (Figure 5C). In binding to the left-hand molecule in Figure 5C, $Spitz_{EGF}$ (magenta) has wedged itself between domain I (blue) and domain III (yellow), causing domain II (green) to become distorted or 'bent'. The amino-terminal part of domain II in the left-hand molecule effectively 'collapses' onto its unaltered counterpart (grey) in the right-hand molecule, creating an additional set of intimate interfacial contacts (Figure 5D). The equivalent domain II regions are splayed apart in the symmetric unligated s-dEGFRΔV dimer (Figure 5B), presumably restrained by direct interactions between domains I and III of the receptor (Figure S1) that we previously suggested may play an autoinhibitory role (Alvarado et al., 2009). The additional >1,000 $Å^2$ of surface area buried in the asymmetric dimer is likely to account for the 30-fold (~ 2 kcal/mole) increase in dimerization affinity observed upon ligand binding.

Formation of the more extensive asymmetric dimer interface seen in Figure 5D arises largely from a ligand-induced kink (of ~12) between modules m4 and m5 of domain II (marked with an arrow in Figure 5B). Modules m2, m3 and m4 from domain II of the left-hand molecule (green) dock onto the domain II surface (grey) of the neighboring molecule in the dimer, without substantially altering the dimerization arm contacts (mediated by module m5). Side-chains from Q189 and R201 (in module m2), plus H205 (in module m3) of the ligand-bound receptor molecule make polar contacts across the dimer interface. Several additional side-chains, including those from P188 and P200 (from module m2) plus L206 and F207 (from module m3) also make van der Waal's contacts with the opposing domain II in Figure 5D. Modules m2, m3, and m4 bury a combined surface of 1,160 $Å^2$ in the asymmetric s-dEGFRΔV dimer interface (34% of the total interface), allowing an intimate set of receptor • receptor contacts to extend along much of the length of domain II in this dimer. Interestingly, Q189, P200, and H205 are conserved in hEGFR and human ErbB3. Q189 is also conserved in hErbB4, P200 in ErbB2, and H205 in hErbB2 and hErbB4. R201, L206 and F207 are not conserved in the human receptors.

Whereas the domain II amino-termini make intimate contacts across the interface of the $(Spitz_{EGF})_2$ • $(s\text{-}dEGFR\Delta V)_2$ dimer, they contribute little to receptor • receptor contacts in the symmetric human sEGFR dimer (Figure 1B), burying just 476 $Å^2$ (with no contribution from m4). Dimerization arm-mediated interactions are very similar in both *Drosophila* and human sEGFR dimers (Garrett et al., 2002; Ogiso et al., 2002). However, additional differences between dEGFR and hEGFR are seen for interactions involving the carboxy-terminal part of domain II (modules m7 and m8). These modules make no direct contact across the interface in ligated human sEGFR dimers, whereas in s-dEGFRΔV they interact more extensively in the unligated dimer than in the ligand-induced dimer. As a result (and because of changes in the domain II/III relationship), ligand binding actually increases the

distance separating the two copies of domain IV in the s-dEGFRΔV dimer by approximately 24 Å (Figures 5A and 5C); *i.e.* ligand binding actually appears to drive apart domains IV of the two receptor molecules in the transition from a putative 'pre-formed dimer' (Figure 5A) to a ligand-activated form (Figure 5C).

A Structural Model for Negative Cooperativity in an EGFR Extracellular Region

Levitzki et al. (1971) pointed out four possible sources for half-of-the-sites reactivity in dimeric enzymes. In the first, the two ligand-binding sites are adjacent such that occupation of one site directly occludes the second. This cannot explain negative cooperativity in EGFR, where the two binding sites in the dimer are more than 50 Å apart. Two other models require non-identical binding sites in unligated dimers that arise either from asymmetric dimerization without ligand or from the existence of distinct subunit classes – neither of which are relevant for dEGFR. The fourth and final model involves a symmetric unligated dimer with two identical binding sites. Ligand binding to one of these sites induces conformational changes that promote asymmetry in the dimer, and restrain the vacant binding site so that its affinity for ligand is reduced. A model of this sort may explain the ligand-binding properties of dEGFR, as illustrated by the gallery of structures presented in Figure 6.

Before interacting with $Spitz_{EGF}$, the ligand-binding sites are identical in crystallographic pre-formed dimers, and presumably monomers, of s-dEGFR (Figure 6A). Ligand may bind to either species. In either case, the first (highest affinity) binding event yields the singly-ligated, asymmetric $Spitz_{EGF}$ • $(s\text{-}dEGFR\Delta V)_2$ dimer shown in Figure 6B. High-affinity ligand binding appears to require receptor dimerization, since the $s\text{-}dEGFR^{dim\text{-}arm}$ mutant shows only low affinity $Spitz_{EGF}$ binding (Figure 3). Indeed, formation of the asymmetric interface in Figure 5D will facilitate domain II bending in the left hand molecule, in turn promoting the wedging apart of domains I and III by the first ligand that binds – and enhancing its affinity.

In the asymmetric s-dEGFRΔV dimer formed after the first (high-affinity) binding event (Figure 6B), domain II in the unoccupied receptor is subjected to a new set of structural restraints. It can no longer 'bend' to allow $Spitz_{EGF}$ to wedge itself fully into the unoccupied ligand-binding site without disrupting the intimate asymmetric interface between amino-terminal parts of domain II shown in Figure 5D. This interface therefore restricts binding of ligand to the right-hand (unligated) receptor in Figure 6B. When a second ligand molecule does bind to the empty site in this dimer, two scenarios (at the extremes) are possible:

- **i.** The asymmetric dimerization interface seen in Figure 6B may be left intact. With the conformation of domain II fixed in the right-hand molecule so that it cannot bend, it will not be possible for a ligand to wedge domains I and III apart upon binding. This restriction will necessitate binding of ligand to an unaltered (suboptimal) site – as seen for $Spitz_{EGF}$ binding to the red binding site in Figure 2A. This would explain the reduced binding affinity of the second (right-hand) site in the s-dEGFR dimer.
- **ii.** Alternatively, ligand binding to the second site in the dimer could wedge domains I and III apart exactly as in the first ligand binding event. The resulting domain II distortion would break the 'extra' contacts in the asymmetric domain II • domain II interface shown in Figure 5D, effectively 'resymmetrizing' the dimer. The work required to disrupt the asymmetric domain II • domain II interface will reduce the effective affinity of the second site for ligand.

The first of these possibilities is likely to explain why asymmetry is maintained in the $(Spitz_{EGF})_2$ • $(s\text{-}dEGFR\Delta V)_2$ dimer even after binding of the second ligand (Figure 6C). The

energetic cost of disrupting the asymmetric dimer interface in Figure 6B presumably outweighs the gain in ligand • receptor interactions that can be achieved by wedging apart domains I and III to optimize the second binding site. The second $Spitz_{EGF}$ molecule therefore binds without altering the s-dEGFRΔV structure, and occupies a compromised binding site (red in Figure 2A) with reduced contact area and fewer predicted hydrogen bonds (and therefore lower affinity). The ~12-fold reduced receptor-binding affinity of $Spitz_{EGF\Delta C}$ appears to prevent this ligand variant from occupying this compromised binding site altogether in our crystals, explaining the half-of-the-sites reactivity seen in the $Spitz_{EGF\Delta C}$ • $(s\text{-}dEGFR\Delta V)_2$ dimer (Figure 4).

The second of the possibilities outlined above is likely to explain the symmetry of the fully occupied human s-EGFRΔIV dimer illustrated in Figure 6D (Ogiso et al., 2002). If domain II-mediated interactions in the asymmetric (singly-ligated) dimer are weaker in human EGFR than in *Drosophila*, they will be disrupted more readily by binding of a second ligand molecule. There are several reasons to suspect that these interactions are indeed weaker in human EGFR than in its *Drosophila* counterpart. Whereas the isolated extracellular region of dEGFR retains negatively cooperative ligand binding, contributions from the intracellular region are essential in the case of human EGFR (Livneh et al., 1986; Macdonald-Obermann and Pike, 2009). This argues that cytoplasmic domain interactions are required to stabilize the singly-ligated intact human EGFR dimers required for negatively cooperative EGF binding. Unlike its *Drosophila* counterpart, isolated s-hEGFR does not form singly-ligated dimers in solution and does not exhibit negatively cooperative ligand binding (Lemmon et al., 1997; Odaka et al., 1997). However, negative cooperativity can be recapitulated in solution by fusing s-hEGFRΔIV to a dimeric IgG Fc domain (Adams et al., 2009) – as also described for the insulin receptor (Bass et al., 1996; Hoyne et al., 2000). Studies of such artificial dimers may be needed in order to examine structural details of the singly-ligated hEGFR dimer inferred from cellular studies. It is also important to note that the intracellular regions of human EGFR and ErbB4 form asymmetric dimers (Jura et al., 2009; Qiu et al., 2008; Red Brewer et al., 2009), which may contribute to the stabilization of asymmetric, singly-ligated dimers of the intact receptors. Residues in this intracellular dimer interface are not conserved in dEGFR, consistent with an increased reliance on extracellular interactions for negative cooperativity in *Drosophila*.

Implications for the High- and Low-Affinity Binding Sites for Human EGF

Our studies suggest that the proposed ‘high-affinity’ and ‘low-affinity’ classes of EGF binding site at the cell surface do not reflect distinct EGFR populations. Rather, the characteristic curved Scatchard plots reflect negatively cooperative EGF binding to a single type of receptor species. In the binding scheme illustrated in Figure 6, the first binding event – leading to the singly-ligated dimer in Figure 6B – could be considered as the ‘high-affinity’ site, and the second (leading to Figure 6C) the ‘low-affinity’ site. Restraints imposed on the second binding site in an asymmetric, singly-ligated dimer can explain negatively cooperative ligand binding in a model that closely resembles mechanisms of negative cooperativity and half-of-the-sites reactivity reported for other multisubunit enzyme systems (Koshland, 1996;Levitzki et al., 1971).

We suggest that studies of the isolated human EGFR extracellular region have failed to recapitulate key receptor-receptor interactions required for its allosteric regulation. Intact human EGFR is reported to self-associate to some extent even in the absence of ligand (Chung et al., 2010; Saffarian et al., 2007), and is thought to form singly-ligated, asymmetric dimers required for negatively cooperative ligand binding at the cell surface (Macdonald and Pike, 2008). Both of these properties are lost when the human EGFR extracellular region is studied in isolation (Lemmon et al., 1997; Odaka et al., 1997). A similar problem exists for the insulin receptor, where negative cooperativity in insulin

binding is completely abolished when the extracellular region of the receptor is released from the membrane surface (De Meyts and Whittaker, 2002). By contrast, the isolated extracellular region of the *Drosophila* EGFR appears to maintain the self-association and allosteric properties of the intact receptor, allowing our studies of s-dEGFR to provide serendipitous insight into the mechanism of its allosteric regulation and structural basis for negative cooperativity.

Conclusions and Perspectives

The origin of concave-up Scatchard plots seen for EGF binding to its cell surface receptor over the past three decades has been contentious. The molecular nature of the 'high-affinity' and 'low-affinity' EGF-binding sites suggested by these curves has also been a subject of significant debate, although recent work suggests that they reflect negative cooperativity rather than distinct classes of site (Macdonald and Pike, 2008). The studies described here provide a structural basis for understanding negative cooperativity in ligand binding to an EGF receptor. Our analysis suggests that high- and low-affinity binding sites for ligand do exist, but that they both occur in the same dimeric receptor complexes and arise from negative cooperativity rather than from distinct populations or 'classes' of receptor.

If the curved Scatchard plots seen in studies of cell surface EGF binding reflect negative cooperativity, how can apparent functional and structural differences between the presumed high-affinity and low-affinity classes of EGF receptors be explained? Early studies with antibodies reported to interfere only with high-affinity or low-affinity sites respectively concluded that the high-affinity subclass is necessary for early signaling responses to EGF (Bellot et al., 1990; Defize et al., 1989). Moreover, the route of EGFR internalization from the cell surface depends on the concentration of ligand used to activate the receptor, suggesting that the high-affinity and low-affinity classes of receptor may be subjected to different endocytic mechanisms (Sorkin and Goh, 2009). At low EGF concentrations, EGFR internalization is primarily clathrin-mediated, whereas clathrin-independent mechanisms appear to dominate when very high EGF concentrations are applied. The negative cooperativity model of Macdonald and Pike (2008) suggests that binding of the second ligand to an EGFR dimer reduces the affinity of the two receptors for one another by ~10-fold. Indeed, our s-dEGFR structures show how the second ligand-binding event must either compromise ligand/receptor or receptor/receptor contacts (Figure 6). A weakened, doubly occupied, EGFR dimer could behave quite differently from one with only one site occupied – with altered dynamics and interaction (and dimer exchange) properties that might alter specificity, degree of autophosphorylation, mechanism of internalization, and other outcomes.

Differences in the signaling properties of singly- and doubly- occupied receptors may also explain the distinct biological outcomes when cells are treated with different agonists for the same ErbB receptor (Wilson et al., 2009), or different concentrations of ligand. For example, EGFR agonists with low receptor-binding affinities (amphiregulin, epiregulin and epigen) might induce the formation of only (or primarily) singly-ligated dimers, whereas EGFR agonists with high affinity for the receptor (EGF, TGFα, betacellulin and HB-EGF) should be able to occupy both binding sites in the receptor dimer if present at sufficiently high concentrations. As a result, the receptor may be activated (and internalized – and ultimately deactivated) differently in response to the two ligand classes. A difference in signaling outcomes of this sort may be very important where EGFR ligands function as morphogens. Gradients of ligands for the *Drosophila* EGFR (Spitz, Keren, Gurken, and Vein) function in tissue patterning in many developmental programs in *D. melanogaster* (Shilo, 2005). It is not clear how different concentrations of these ligands in morphogen gradients can induce different cell fates, which is crucial for 'interpreting' the gradients. Our work suggests one possibility. At the gradient peak, where ligand concentrations are high, dEGFR dimers will

be fully occupied (with 2 ligands bound per dimer). By contrast, at the tail end of the morphogen gradient where ligand concentrations are low, only high-affinity sites will be occupied in the receptor dimers – yielding singly-ligated dEGFR dimers. If the doubly- and singly-ligated dimers have different signaling properties and internalization routes, distinct cell fates could be induced in the two regimes of receptor activation. This graded occupation of the two binding sites in the EGFR dimer would be substantially lessened in a non-cooperative system.

EXPERIMENTAL PROCEDURES

Protein expression and purification

Histidine-tagged s-dEGFR proteins were produced by secretion from baculovirus-infected Sf9 cells and purified exactly as described (Alvarado et al., 2009). An Avi tag-encoding sequence was included after the C-terminal histidine tag (see Supplemental Information) for biotinylating protein for fluorescent ligand binding assays. $Spitz_{EGF}$ and $Spitz_{EGF\Delta C}$ were secreted from stably-transfected *Drosophila* Schneider-2 (S2) cells and purified as described in Supplemental Information.

Crystallography

Crystals of the $(Spitz_{EGF})_2$ • $(s\text{-}dEGFR\Delta V)_2$ dimer were obtained using the hanging drop method, mixing equal volumes of protein (75 μM s-dEGFRΔV, 90 μM $Spitz_{EGF}$) and reservoir solution (1.5 M $NaKPO_4$, pH 6.9, with 4% t-butanol), and equilibrating over this reservoir at 21 C. Crystals grew to ~0.5 × 0.3 × 0.15 mm, and were cryoprotected by adding stepwise to the drop sodium malonate, pH 6.9 (mixed with reservoir solution) until a sodium malonate concentration was reached (1.7–2 M) that allowed the solution to freeze clear. Frozen crystals diffracted to 3.2 Å resolution at CHESS beamline F1, and belonged to space group $P2_12_12_1$ with unit cell dimensions a=118.2 Å; b=124.2 Å; c=186.5 Å (Table S1). The asymmetric unit contained two s-dEGFRΔV molecules, with solvent content of 70.1%.

$Spitz_{EGF\Delta C}$ • $(s\text{-}dEGFR\Delta V)_2$ dimer crystals (up to 0.5 × 0.2 × 0.2 mm) grew at 21 C using the hanging drop method, from a mixture of purified s-dEGFRΔV (50 μM) and $Spitz_{EGF\Delta C}$ (60 μM) and reservoir solution (11% PEG 20,000, 0.1 M HEPES, pH 7.4, with 3% n-propanol). Prior to freezing in liquid nitrogen, crystals were cryoprotected by adding ethylene glycol (in 13% PEG 20,000 and 0.1M HEPES, pH 7.4) stepwise a final concentration in the drop of 30% (v/v). Crystals diffracted to 3.4 Å resolution at APS beamline 23-ID-D, and belonged to space group $P2_12_12_1$, with unit cell dimensions a=73.8 Å, b=120.2 Å, c=274.7 Å (Table S1). With one receptor:ligand (2:1) complex in the asymmetric unit, solvent content is 68.7%. Diffraction data for $Spitz_{EGF\Delta C}$ • $(s\text{-}dEGFR\Delta V)_2$ crystals were visibly anisotropic, and were subjected to ellipsoidal truncation to 4 Å in the a^* axis and 3.5 Å in the b^* and c^* axes, and anisotropic scaling (http://www.doe-mbi.ucla.edu/~sawaya/anisoscale/) (Strong et al., 2006).

Data were processed with the program HKL2000 (Otwinowski and Minor, 1997), and structures solved by molecular replacement (MR) using the program Phaser (CCP4, 1994). An MR solution for one molecule in the receptor dimer was found readily for both datasets using coordinates from unligated s-dEGFRΔV (PDB code 3I2T) as the search model. The resulting maps showed clear electron density for the second receptor molecule and its bound $Spitz_{EGF}$ or $Spitz_{EGF\Delta C}$ molecule, allowing domains I and III to be placed and domains II and IV to be fit. Initial fitting focused on the $Spitz_{EGF\Delta C}$ • $(s\text{-}dEGFR\Delta V)_2$ dimer structure, early models of which were used to improve model phases for the $Spitz_{EGF}$/s-dEGFRΔV complex. Cycles of manual building/rebuilding using COOT (Emsley and Cowtan, 2004) were alternated with rounds of refinement employing REFMAC and solvent flattening with

the program DM (CCP4, 1994), plus composite omit maps calculated with CNS (Brünger et al., 1998). TLS refinement (Winn et al., 2001) was used in later stages, using REFMAC (CCP4, 1994), with anisotropic motion tensors refined for each of the receptor domains and bound ligand molecules.

Although initial maps for the $Spitz_{EGF\Delta C}$ • $(s\text{-}dEGFR\Delta V)_2$ complex showed clear density for the second receptor molecule and its bound $Spitz_{EGF\Delta C}$ molecule, the quality of the electron density remained poor throughout large areas of this structure during refinement and phase combination, particularly in domains I and III. We therefore re-solved this structure by MR using the refined (receptor-only) coordinates of each receptor molecule in the $(Spitz_{EGF})_2$ • $(s\text{-}dEGFR\Delta V)_2$ complex as independent search models in sequential steps. Both receptor molecules were found readily with Phaser (CCP4, 1994), and clear $Spitz_{EGF\Delta C}$ density in only one binding site (Figure 4) allowed its placement as a rigid body. The coordinates for the MR search model (plus placed ligand) were then subjected only to rigid body refinement, with each receptor domain (and single placed ligand) as an independent body. R/R_{free} values of 41.0/42.7 were obtained (Table S1). Structural figures were generated using PyMol (DeLano, 2002).

Receptor biotinylation and fluorescent ligand binding assays

Purified s-dEGFR and $s\text{-}dEGFR^{dim\text{-}arm}$ were biotinylated, and $Spitz_{EGF}$ was fluorescently labled with AlexaFluor-488 using standard procedures detailed in Supplemental Information. Biotinylated s-dEGFR was captured in Reacti-Bind streptavidin-coated 96-well plates (Pierce) in TBS plus 0.5% (w/v) bovine serum albumin (TBS-B). Labeled $Spitz_{EGF}$ in TBS-B was then added at a range of concentrations, both to wells with biotinylated s-dEGFR protein and mock-treated wells, and agitated at 25 C for 2 h. Total ligand fluorescence per well was then counted in a Tecan Safire-2 microplate reader. The plate was then quickly washed with TBS-B, and the remaining (bound) fluorescent ligand was measured. Specific binding was determined by subtracting from the fluorescence measured for each well containing bound s-dEGFR protein the background fluorescence measured for mock-treated wells subjected to the same labeled $Spitz_{EGF}$ concentration. Background was typically less than 10% of the binding signal for s-dEGFR experiments, and less than 50% (at low ligand concentrations) for $s\text{-}dEGFR^{dim\text{-}arm}$ experiments. Fluorescence values for (specifically) bound labeled (and free) $Spitz_{EGF}$ were converted to picomoles using a standard curve generated by measuring fluorescence of known labeled $Spitz_{EGF}$ concentrations.

Supplementary Material

Refer to Web version on PubMed Central for supplementary material.

Acknowledgments

We thank Kate Ferguson, Jim Shorter, Jason Davis, Greg Van Duyne, Ben Black, Steve Stayrook and members of the Lemmon and Ferguson laboratories for valuable comments. Crystallographic data were collected at Cornell High Energy Synchrotron Source (CHESS) beamline F1, supported by the NSF and NIH/NIGMS under NSF award DMR-0225180, using the Macromolecular Diffraction at CHESS (MacCHESS) facility supported by the NCRR (RR-01646). Additional data were collected at the GM/CA Collaborative Access Team at the Advanced Photon Source (APS), funded by the NCI (Y1-CO-1020), NIGMS (Y1-GM-1104), and the US Department of Energy (contract No. W-31-109-ENG-38). This work was funded by NIH grants R01-CA125432 and R01-CA079992 (M.A.L.), and predoctoral fellowship W81XWH-04-1-0328 from the U.S. Army Breast Cancer Research Program (D.E.K.). D.A. was supported by NIH Postdoctoral Training Grant T32HD007516 and a Postdoctoral Fellowship from the Damon Runyon Cancer Research Foundation (DRG-1884-05). Coordinates and structure factors for $(Spitz_{EGF})_2$ • $(s\text{-}dEGFR\Delta V)_2$ and $Spitz_{EGF\Delta C}$ • $(s\text{-}dEGFR\Delta V)_2$ dimers have been deposited in the Protein Data Bank (www.rcsb.org/pdb) with accession codes 3LTF and 3LTG.

References

Adams TE, Koziolek EJ, Hoyne PH, Bentley JD, Lu L, Lovrecz G, Ward CW, Lee FT, Scott AM, Nash AD, et al. A truncated soluble epidermal growth factor receptor-Fc fusion ligand trap displays anti-tumour activity in vivo. Growth Factors. 2009; 27:141–154. [PubMed: 19333814]

Alvarado D, Klein DE, Lemmon MA. ErbB2 resembles an autoinhibited invertebrate epidermal growth factor receptor. Nature. 2009; 461:287–291. [PubMed: 19718021]

Bass J, Kurose T, Pashmforoush M, Steiner DF. Fusion of insulin receptor ectodomains to immunoglobulin constant domains reproduces high-affinity insulin binding in vitro. J Biol Chem. 1996; 271:19367–19375. [PubMed: 8702623]

Bellot F, Moolenaar W, Kris R, Mirakhur B, Verlaan I, Ullrich A, Schlessinger J, Felder S. High-affinity epidermal growth factor binding is specifically reduced by a monoclonal antibody, and appears necessary for early responses. J Cell Biol. 1990; 110:491–502. [PubMed: 2298813]

Bouyain S, Longo PA, Li S, Ferguson KM, Leahy DJ. The extracellular region of ErbB4 adopts a tethered conformation in the absence of ligand. Proc Natl Acad Sci U S A. 2005; 102:15024–15029. [PubMed: 16203964]

Brünger AT, Adams PD, Clore GM, DeLano WL, Gros P, Grosse-Kunstleve RW, Jiang JS, Kuszewski J, Nilges M, Pannu NS, et al. Crystallography & NMR system: A new software suite for macromolecular structure determination. Acta Crystallogr D Biol Crystallogr. 1998; 54:905–921. [PubMed: 9757107]

Burgess AW, Cho HS, Eigenbrot C, Ferguson KM, Garrett TP, Leahy DJ, Lemmon MA, Sliwkowski MX, Ward CW, Yokoyama S. An open-and-shut case? Recent insights into the activation of EGF/ErbB receptors. Mol Cell. 2003; 12:541–552. [PubMed: 14527402]

CCP4 (Collaborative Computational Project Number 4). The CCP4 suite: Programs for protein crystallography. Acta Crystallogr D Biol Crystallogr. 1994; 50:760–763. [PubMed: 15299374]

Cho HS, Leahy DJ. Structure of the extracellular region of HER3 reveals an interdomain tether. Science. 2002; 297:1330–1333. [PubMed: 12154198]

Chung I, Akita R, Vandlen R, Toomre D, Schlessinger J, Mellman I. Spatial control of EGF receptor activation by reversible dimerization on living cells. Nature. 2010; 464:783–787. [PubMed: 20208517]

De Meyts P, Whittaker J. Structural biology of insulin and IGF1 receptors: implications for drug design. Nat Rev Drug Discov. 2002; 1:769–783. [PubMed: 12360255]

Defize LH, Boonstra J, Meisenhelder J, Kruijer W, Tertoolen LG, Tilly BC, Hunter T, van Bergen en Henegouwen PM, Moolenaar WH, de Laat SW. Signal transduction by epidermal growth factor occurs through the subclass of high affinity receptors. J Cell Biol. 1989; 109:2495–2507. [PubMed: 2553748]

DeLano, WL. The PyMOL Molecular Graphics System. Palo Alto, CA, USA: DeLano Scientific; 2002.

Emsley P, Cowtan K. Coot: model-building tools for molecular graphics. Acta Crystallogr D Biol Crystallogr. 2004; 60:2126–2132. [PubMed: 15572765]

Ferguson KM. Structure-Based View of Epidermal Growth Factor Receptor Regulation. Annu Rev Biophys. 2008; 37:353–373. [PubMed: 18573086]

Ferguson KM, Berger MB, Mendrola JM, Cho HS, Leahy DJ, Lemmon MA. EGF activates its receptor by removing interactions that autoinhibit ectodomain dimerization. Mol Cell. 2003; 11:507–517. [PubMed: 12620237]

Garrett TP, McKern NM, Lou M, Elleman TC, Adams TE, Lovrecz GO, Zhu HJ, Walker F, Frenkel MJ, Hoyne PA, et al. Crystal structure of a truncated epidermal growth factor receptor extracellular domain bound to transforming growth factor alpha. Cell. 2002; 110:763–773. [PubMed: 12297049]

Groenen LC, Nice EC, Burgess AW. Structure-function relationships for the EGF/TGF-alpha family of mitogens. Growth Factors. 1994; 11:235–257. [PubMed: 7779404]

Hoyne PA, Cosgrove LJ, McKern NM, Bentley JD, Ivancic N, Elleman TC, Ward CW. High affinity insulin binding by soluble insulin receptor extracellular domain fused to a leucine zipper. FEBS Letts. 2000; 479:15–18. [PubMed: 10940380]

Hynes NE, MacDonald G. ErbB receptors and signaling pathways in cancer. Curr Opin Cell Biol. 2009; 21:177–184. [PubMed: 19208461]

Jorissen RN, Walker F, Pouliot N, Garrett TP, Ward CW, Burgess AW. Epidermal growth factor receptor: mechanisms of activation and signalling. Exp Cell Res. 2003; 284:31–53. [PubMed: 12648464]

Jura N, Endres NF, Engel K, Deindl S, Das R, Lamers MH, Wemmer DE, Zhang X, Kuriyan J. Mechanism for activation of the EGF receptor catalytic domain by the juxtamembrane segment. Cell. 2009; 137:1293–1307. [PubMed: 19563760]

Klein P, Mattoon D, Lemmon MA, Schlessinger J. A structure-based model for ligand binding and dimerization of EGF receptors. Proc Natl Acad Sci U S A. 2004; 101:929–934. [PubMed: 14732694]

Koshland DE Jr. The structural basis of negative cooperativity: receptors and enzymes. Curr Opin Struct Biol. 1996; 6:757–761. [PubMed: 8994875]

Lax I, Mitra AK, Ravera C, Hurwitz DR, Rubinstein M, Ullrich A, Stroud RM, Schlessinger J. Epidermal growth factor (EGF) induces oligomerization of soluble, extracellular, ligand-binding domain of EGF receptor. A low resolution projection structure of the ligand-binding domain. J Biol Chem. 1991; 266:13828–13833. [PubMed: 1856216]

Lemmon MA. Ligand-induced ErbB receptor dimerization. Exp Cell Res. 2009; 315:638–648. [PubMed: 19038249]

Lemmon MA, Bu Z, Ladbury JE, Zhou M, Pinchasi D, Lax I, Engelman DM, Schlessinger J. Two EGF molecules contribute additively to stabilization of the EGFR dimer. EMBO J. 1997; 16:281–294. [PubMed: 9029149]

Levitzki A, Stallcup WB, Koshland DE Jr. Half-of-the-sites reactivity and the conformational states of cytidine triphosphate synthetase. Biochemistry. 1971; 10:3371–3378. [PubMed: 4940762]

Livneh E, Prywes R, Kashles O, Reiss N, Sasson I, Mory Y, Ullrich A, Schlessinger J. Reconstitution of human epidermal growth factor receptors and its deletion mutants in cultured hamster cells. J Biol Chem. 1986; 261:12490–12497. [PubMed: 3017977]

Macdonald JL, Pike LJ. Heterogeneity in EGF-binding affinities arises from negative cooperativity in an aggregating system. Proc Natl Acad Sci U S A. 2008; 105:112–117. [PubMed: 18165319]

Macdonald-Obermann JL, Pike LJ. The intracellular juxtamembrane domain of the epidermal growth factor (EGF) receptor is responsible for the allosteric regulation of EGF binding. J Biol Chem. 2009; 284:13570–13576. [PubMed: 19336395]

Magun BE, Matrisian LM, Bowden GT. Epidermal growth factor. Ability of tumor promoter to alter its degradation, receptor affinity and receptor number. J Biol Chem. 1980; 255:6373–6381. [PubMed: 6967066]

Odaka M, Kohda D, Lax I, Schlessinger J, Inagaki F. Ligand-binding enhances the affinity of dimerization of the extracellular domain of the epidermal growth factor receptor. J Biochem. 1997; 122:116–121. [PubMed: 9276679]

Ogiso H, Ishitani R, Nureki O, Fukai S, Yamanaka M, Kim JH, Saito K, Sakamoto A, Inoue M, Shirouzu M, et al. Crystal structure of the complex of human epidermal growth factor and receptor extracellular domains. Cell. 2002; 110:775–787. [PubMed: 12297050]

Otwinowski Z, Minor W. Processing of X-ray diffraction data collected in oscillation mode. Methods Enzymol. 1997; 276:307–326.

Qiu C, Tarrant MK, Choi SH, Sathyamurthy A, Bose R, Banjade S, Pal A, Bornmann WG, Lemmon MA, Cole PA, et al. Mechanism of activation and inhibition of the HER4/ErbB4 kinase. Structure. 2008; 16:460–467. [PubMed: 18334220]

Red Brewer M, Choi SH, Alvarado D, Moravcevic K, Pozzi A, Lemmon MA, Carpenter G. The juxtamembrane region of the EGF receptor functions as an activation domain. Mol Cell. 2009; 34:641–651. [PubMed: 19560417]

Saffarian S, Li Y, Elson EL, Pike LJ. Oligomerization of the EGF receptor investigated by live cell fluorescence intensity distribution analysis. Biophys J. 2007; 93:1021–1031. [PubMed: 17496034]

Schlessinger J. Allosteric regulation of the epidermal growth factor receptor kinase. J Cell Biol. 1986; 103:2067–2072. [PubMed: 3023396]

Schnepp B, Donaldson T, Grumbling G, Ostrowski S, Schweitzer R, Shilo BZ, Simcox A. EGF domain swap converts a drosophila EGF receptor activator into an inhibitor. Genes Dev. 1998; 12:908–913. [PubMed: 9531530]

Sharma SV, Bell DW, Settleman J, Haber DA. Epidermal growth factor receptor mutations in lung cancer. Nat Rev Cancer. 2007; 7:169–181. [PubMed: 17318210]

Shilo BZ. Regulating the dynamics of EGF receptor signaling in space and time. Development. 2005; 132:4017–4027. [PubMed: 16123311]

Shoyab M, De Larco JE, Todaro GJ. Biologically active phorbol esters specifically alter affinity of epidermal growth factor membrane receptors. Nature. 1979; 279:387–391. [PubMed: 16068160]

Sorkin A, Goh LK. Endocytosis and intracellular trafficking of ErbBs. Exp Cell Res. 2009; 315:683–696. [PubMed: 19278030]

Strong M, Sawaya MR, Wang S, Phillips M, Cascio D, Eisenberg D. Toward the structural genomics of complexes: crystal structure of a PE/PPE protein complex from Mycobacterium tuberculosis. Proc Natl Acad Sci U S A. 2006; 103:8060–8065. [PubMed: 16690741]

Wilson KJ, Gilmore JL, Foley J, Lemmon MA, Riese DJ 2nd. Functional selectivity of EGF family peptide growth factors: implications for cancer. Pharmacol Ther. 2009; 122:1–8. [PubMed: 19135477]

Winn MD, Isupov MN, Murshudov GN. Use of TLS anisotropic displacements in macromolecular refinement. Acta Crystallogr D Biol Crystallogr. 2001; 57:122–133. [PubMed: 11134934]

Wofsy C, Goldstein B, Lund K, Wiley HS. Implications of epidermal growth factor (EGF) induced egf receptor aggregation. Biophys J. 1992; 63:98–110. [PubMed: 1420877]

Yarden Y, Schlessinger J. Epidermal growth factor induces rapid, reversible aggregation of the purified epidermal growth factor receptor. Biochemistry. 1987; 26:1443–1451. [PubMed: 3494473]

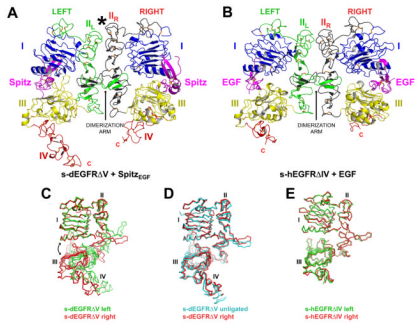

FIGURE 1. An Asymmetric Ligand-Induced s-dEGFRΔV Dimer

(A) The $(Spitz_{EGF})_2$ • $(s\text{-}dEGFR\Delta V)_2$ dimer is asymmetric. Domains I, III, and IV are blue, yellow and red respectively. Domain II is green in the left-hand molecule (II_L) and dark grey in the right-hand molecule (II_R). Bound ligand is magenta. The domain II dimerization arm is labeled. An asterisk marks the amino-terminal part of domain II where asymmetry is most evident.

(B) Structure (PDB code 1IVO) of the symmetric EGF-induced dimer of the human EGFR extracellular region (s-hEGFR) lacking domain IV (Ogiso et al., 2002), colored as in (A).

(C) Overlay of the left (green) and right (red) molecules from the s-dEGFRΔV dimer, using domain I as reference. A double-headed curved arrow illustrates 'wedging' apart of domains I and III in the green molecule compared with the red molecule, breaking direct domain I/III interactions detailed in Figure S1, and altering the domain II conformation so that the dimerization arm is substantially reoriented.

(D) Overlay of the right-hand molecule from the asymmetric s-dEGFRΔV dimer (red) on unligated s-dEGFRΔV (cyan) from PDB code 3I2T (Alvarado et al., 2009), using domain I as reference.

(E) Overlay of the two receptor molecules in the human $(EGF)_2$ • $(s\text{-}hEGFR\Delta IV)_2$ dimer. See Table S1 for crystallographic statistics.

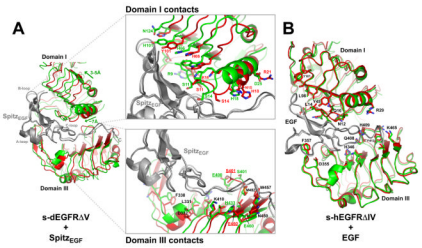

FIGURE 2. The Ligand-Binding Sites in the $(Spitz_{EGF})_2$• (s-dEGFRΔV)$_2$ Dimer are Inequivalent

(A) Overlay of the two ligands (grey) in the $(Spitz_{EGF})_2$ • (s-dEGFRΔV)$_2$ dimer, illustrating differences in their binding sites (see also Figure S2). The green structure corresponds to the left-hand molecule in Figure 1A, and the red structure to the right-hand molecule. Green arrows denote the ~3–5 Å shift of the green domain I towards the top left of the figure and the ~7 Å translation of the N-terminal helix described in the text. A-, B-, and C-loops of the bound ligand are labeled. The upper insert details s-dEGFRΔV side-chains that interact with $Spitz_{EGF}$, highlighting significant changes. The lower insert gives a similar view of domain III interactions which are only modestly changed. Residues underlined (E400, S401, H433 and E460) are mentioned in the text.

(B) Analogous overlay of the two bound ligands in the human $(EGF)_2$ • (s-hEGFRΔIV)$_2$ dimer from Figure 1B (Ogiso et al., 2002), illustrating similarity of the two binding sites. Most side chains that contact bound ligand overlay very well in this superimposition.

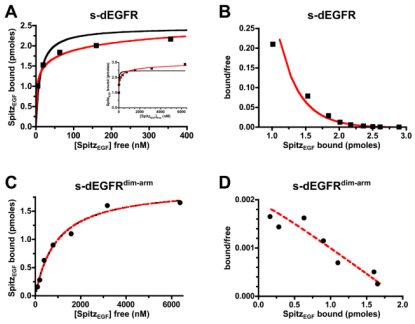

FIGURE 3. $Spitz_{EGF}$ Binding to s-dEGFR Yields Curved Scatchard Plots

(A) Experimental data for binding of fluorescently-labeled $Spitz_{EGF}$ to biotinylated s-dEGFR are well fit by the Hill equation with a Hill coefficient (n_H) of 0.31 (red curve), but not a simple hyperbola (black). The inset shows saturation at >6 μM $Spitz_{EGF}$. Data are representative of over six independent experiments.

(B) Scatchard transformation of binding data shown in (A). The characteristic concave-up curvature is fit well by the Hill equation (n_H = 0.31) – suggesting negative cooperativity.

(C) Data for fluorescent $Spitz_{EGF}$ binding to a dimerization-defective s-dEGFR variant (s-$dEGFR^{dim\text{-}arm}$) are well fit by a simple hyperbolic binding curve (black) or by the Hill equation with Hill coefficient of 1.02, suggesting no cooperativity. Data are representative of over six independent experiments.

(D) Scatchard transformation of data shown in (C) yields a straight line, arguing that s-dEGFR dimerization is required for negative cooperativity.

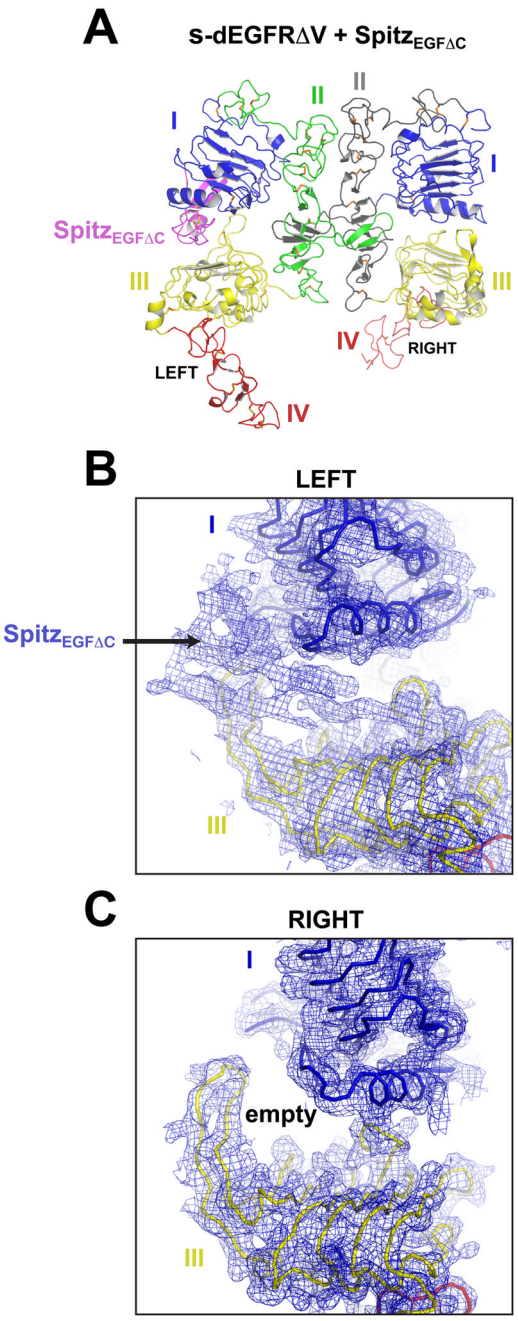

FIGURE 4. Half-of-the-Sites Reactivity in s-dEGFRΔV

(A) Crystal structure of an s-dEGFRΔV dimer bound to $Spitz_{EGFΔC}$. Ligand is bound to the left-hand molecule in which domains I and III are 'wedged' apart, but not the right-hand receptor molecule, which structurally resembles unligated s-dEGFRΔV. $Spitz_{EGFΔC}$ lacks six amino acids from its C-terminus, and binds s-dEGFRΔV with apparent K_D = 4.37 ± 0.26 μM, 12-fold weaker than the value of 368 ± 23 nM measured for $Spitz_{EGF}$ (Figure S3). (B) Electron density is shown from a $2F_o$-F_c map (blue) contoured at 1.0σ, calculated with model phases from the receptor molecules alone. In the region corresponding to the left-hand binding site in (A), clear density for bound ligand is seen. Cα traces for domains I and

III are shown in blue and yellow respectively in the density, and the small part of domain IV seen is red.

(C) By contrast, the $2F_o$-F_c map suggests no density for bound ligand in the region corresponding to the right-hand binding site in (A). This binding site appears to be vacant in crystals of a $Spitz_{EGF\Delta C}$ • (s-dEGFRΔV)$_2$ dimer.

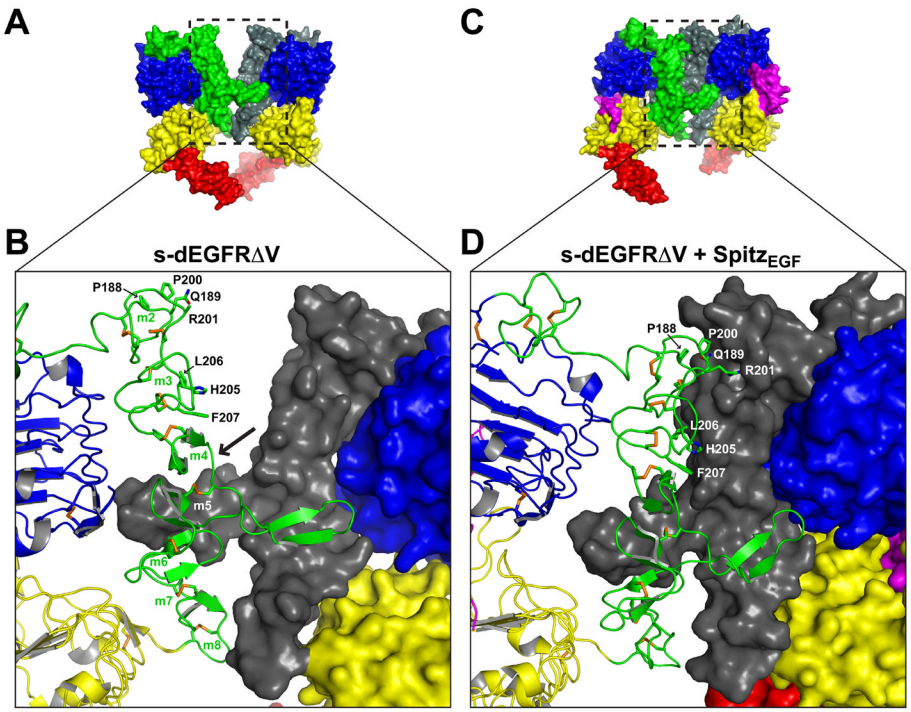

FIGURE 5. Ligand Binding Promotes an Extensive Asymmetric Dimerization Interface

(A) Crystallographic dimer of unligated s-dEGFRΔV reported previously (Alvarado et al., 2009), shown surface-rendered with individual domains colored as in Figure 1A.

(B) Close-up of the unligated s-dEGFRΔV dimer in the domain II region. Disulfide-bonded modules m2 to m8 are labeled, as are selected residues that interact across the ligated dimer interface in (D). An arrow marks the location between modules m4 and m5 of the ligand-induced kink (of ~12) that allows the amino-terminal region of the left-hand domain II to 'collapse' intoits right-hand counterpart in (D).

(C) Surface rendered asymmetric $(Spitz_{EGF})_2$ • $(s\text{-}dEGFR\Delta V)_2$ dimer, with individual domains and ligand colored as in (A).

(D) Domain II region close-up of the $(Spitz_{EGF})_2$ • $(s\text{-}dEGFR\Delta V)_2$ dimer. Disulfide-bonded modules m2, m3 and m4 from the left-hand molecule (green) have 'collapsed' onto their counterparts in the right-hand molecule (grey), burying 1,160 $Å^2$ in an intimate domain II interface. Dimerization arm-mediated contacts are largely unaltered.

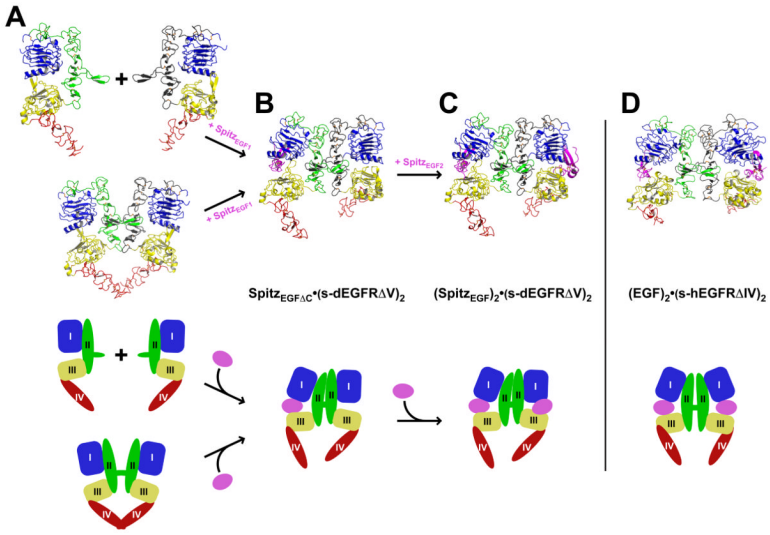

FIGURE 6. Model for Negatively Cooperative Ligand Binding to s-dEGFR

(A–C) Structures and cartoons describe a model for negatively cooperative ligand binding to s-dEGFRΔV. Domains (and ligand) are colored as in Figure 1.

(A) Binding of a single ligand to either 'pre-formed' s-dEGFRΔV dimers (which have two identical binding sites) or s-dEGFRΔV monomers yields the singly ligated dimer shown in (B).

(B) Singly ligated s-dEGFRΔV dimers are asymmetric. Binding of $Spitz_{EGF\Delta C}$ to the left-hand molecule wedges apart domains I and III (blue and yellow), and thus 'bends' domain II such thatit collapses against its counterpart in the neighboring right-hand molecule, as in Figure 5D.

(C) A second $Spitz_{EGF}$ binds to the singly-ligated dimer, and occupies the binding site in the right-hand molecule with no change in s-dEGFR conformation. The intimate dimer interface in (B) restrains domain II in the right hand molecule, so that domains I and III cannot readily be wedged apart. Thus, the binding event that occurs in going from (B) to (C) involves a compromised set of ligand/receptor interactions as described in Figure 2A, reducing binding affinity (and retaining asymmetry in the doubly-ligated dimer).

(D) The dimer of human sEGFRΔIV formed upon EGF binding is symmetric (Ogiso et al., 2002), with both ligands bound in the same manner (Figure 2B). A symmetric dimer of this sort would form following ligand binding to the dimer in (B) if ligand/receptor contacts were maximized at the expense of contacts in the dimerization interface.